

Stress and fabric evolution in superellipsoid assemblies: influence of particle shape under constant mean stress shearing

Yuxuan Wen¹ and T. Matthew Evans^{2,*}

¹National Key Laboratory for Safety and Resilience of Civil Engineering in Mountain Areas, East China Jiaotong University, Nanchang, China, 330013

²School of Civil and Construction Engineering, Oregon State University, Corvallis, OR, USA 97331

Abstract. The mechanical behavior of granular assemblies is strongly influenced by particle shape, yet many discrete element method (DEM) simulations rely on spheres or ellipsoids to reduce computational overhead and employ well-established stress-force-fabric relationships. Advanced imaging techniques such as X-ray micro-computed tomography (μ CT) are increasingly capable of capturing high-resolution particle geometries but remain expensive and limited in availability. Superellipsoids capture key characteristics of natural particles – such as elongation, triaxiality, and varying surface curvature – through a relatively simple closed-form equation amenable to efficient DEM analysis. Herein, we investigate mixtures of arbitrarily shaped superellipsoids to better approximate the geometric diversity found in real grains and reference behaviour back to assemblies of monoshaped particles. Simulation results highlight that aspect ratio is the primary factor affecting compactivity (i.e., packing efficiency), shear strength, and fabric anisotropy. Spherical particles produce higher void ratios and lower shear strength, whereas more cubic shapes lead to denser packings and stronger force chains. Random distributions of shape parameters (sharpness and squareness) result in higher compactivity and shear strength, yet randomizing aspect ratios has an even more pronounced effect, particularly on fabric anisotropy. These findings underscore the significance of incorporating particle shape heterogeneity in DEM simulations, as an over-reliance on idealized spherical assumptions may underestimate both the compaction behavior and shear strength of granular materials.

1 Introduction

The discrete element method (DEM) is a robust computational tool widely employed for simulating emergent behavior in granular materials across various spatiotemporal scales and under diverse strain rate and stress conditions. Although the fundamental mathematics underpinning DEM is straightforward, the computational demands of simulating particle assemblies at realistic scales remain substantial, primarily due to processor-bound constraints. Consequently, numerous optimization techniques have been introduced to alleviate computational burdens. A prevalent approach involves approximating particles as spheres, significantly simplifying contact detection algorithms and reducing computational overhead associated with particle inertia and orientation calculations. However, particles are generally aspherical, and their shapes are well-known to influence overall assembly behaviour [1-3].

Alternative approaches to modeling realistic particle geometries include techniques such as clumped-spheres [4-6], which introduce unwanted artificial surface roughness and substantially increase the particle count, and polyhedral particles [7-9] whose contact detection efficiency critically depends on the number of vertices.

Compared to these methods, superellipsoids represent an attractive intermediate solution for capturing particle shape in DEM simulations. Superellipsoids allow direct control over angularity, elongation, and flatness, thus encompassing a broad

spectrum of particle geometries through a simple closed-form analytical description. Moreover, efficient contact detection algorithms, such as Levenberg-Marquardt (LM) [10, 11] and Gilbert-Johnson-Keerthi (GJK) [12], remain viable for superellipsoids, enabling relatively rapid computations while accurately preserving essential particle-shape effects [13].

The inside-outside function (implicit function) for a superellipsoid can be expressed analytically as:

$$f(\mathbf{x}; \mathbf{r}, \boldsymbol{\varepsilon}) = \left[\left(\frac{x_1}{r_1} \right)^{\frac{2}{\varepsilon_2}} + \left(\frac{x_2}{r_2} \right)^{\frac{2}{\varepsilon_2}} \right]^{\frac{\varepsilon_2}{\varepsilon_1}} + \left(\frac{x_3}{r_3} \right)^{\frac{2}{\varepsilon_1}} \quad (1)$$

where r_i ($i \in [1,3]$) are the semi-axis lengths, and ε_j ($j \in [1,2]$) are shape exponents controlling squareness and sharpness. Superellipsoid shapes corresponding to variations of ε_1 and ε_2 are illustrated in Fig. 1.

This manuscript presents results from a selection of DEM simulations of assemblies of superellipsoids. Our goal is to briefly highlight the importance of particle shape heterogeneity in DEM simulations and lay the foundation for more detailed future studies of the same.

2 Numerical simulations

Simulations were conducted on assemblies consisting of 10,000 super-ellipsoidal particles. Each simulation was initialized from an identical random point cloud, with particle positions and orientations remaining consistent across all tests. Particles were placed without initial

* Corresponding author: matt.evans@oregonstate.edu

contacts. All assemblies share the same cumulative particle volume distribution, presented here in terms of equivalent sphere diameters, defined as the diameter of spheres having the same volume as the corresponding superellipsoidal particles (Fig. 2).

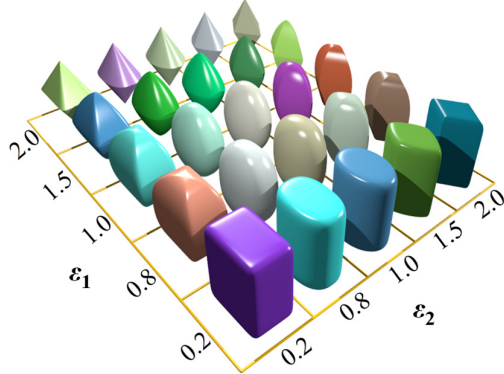


Fig. 1. Superellipsoid shape variation with respect to parameters ϵ_1 (squareness) and ϵ_2 (sharpness) [14]

A linear contact model is adopted for the simulations, with a normal contact stiffness $k_n = 2.4 \times 10^5$ N/m, derived from the relation $k_n/r_0 = 1$ GPa, where r_0 is the mean sphere-equivalent particle radius in the assembly. This choice has been shown to produce results consistent with the Hertz–Mindlin contact law [15], while significantly improving computational efficiency. The shear stiffness is set as $k_s = 0.8k_n$, and the interparticle friction coefficient is 0.5. A numerical damping coefficient of 0.3 is applied following Cundall’s approach.

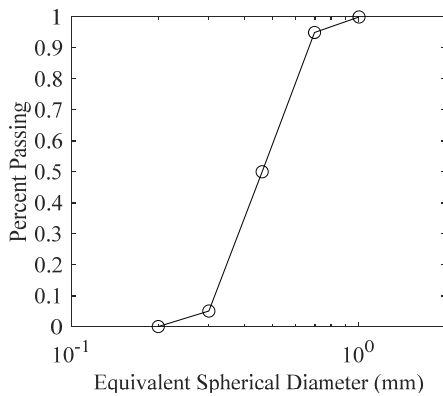


Fig. 2. Particle size distribution (equivalent sphere diameters) used in all simulations.

Simulations were performed on eight assemblies, each containing particles with distinct shape characteristics, as detailed in Table 1. Test 1 serves as the benchmark, consisting solely of spherical particles with varying diameters. Tests 2 to 5 involve superellipsoidal particles with constant shape parameters within each test, but varying particle sizes. To investigate the effect of randomly distributed shape parameters, Tests 6 to 8 were designed. Specifically, in Test 6, the particle semi-axis ratios remain constant at 1:1:1, while shape exponents ϵ_1 and ϵ_2 vary randomly within the specified range. In Test 7, shape exponents are fixed, and the semi-axis length ratios are randomly distributed (i.e., particles are scalene ellipsoids). Test 8 allows random variation of all shape parameters.

Schematic illustrations of particle shapes used in Tests 1 to 5 are presented in Fig. 3.

Table 1. Particle shape characteristics for each simulation.

Test	$r_1 : r_2 : r_3$	ϵ_1	ϵ_2
1	1 : 1 : 1	1.0	1.0
2	1 : 1 : 1	0.6	0.6
3	1 : 1 : 1	1.4	1.4
4	1 : 1 : 1	0.6	1.4
5	1 : 1 : 1	1.4	0.6
6	1 : 1 : 1	0.6 ~ 1.4	0.6 ~ 1.4
7	0.6 ~ 1.4	1.0	1.0
8	0.6 ~ 1.4	0.6 ~ 1.4	0.6 ~ 1.4

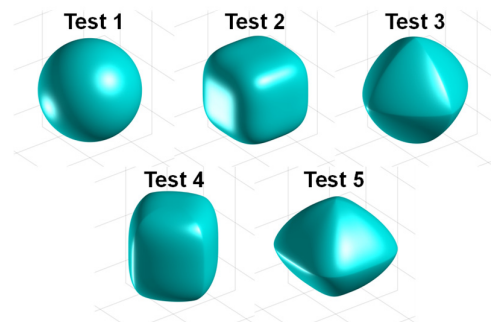


Fig. 3. Particle shapes used in Tests 1 to 5.

The initial particle cloud is generated inside a cube with side length $D = Xd_{50}$ where d_{50} represents the median particle diameter, and the factor X varies from 58.2 to 61.8 across the eight simulations. The assembly is first isotropically consolidated to a mean stress of $p = 100$ kPa by moving all six rigid boundaries inward uniformly. Following consolidation, each specimen is compressed vertically by advancing the top and bottom rigid walls at constant velocity while relaxing the four lateral walls using a numerical servomechanism to maintain a constant mean stress of $p = 100$ kPa. Shearing continues to a global axial strain of 50% is reached.

3 Simulation results

Consolidation curves from the eight tests are presented in Fig. 4. The results show that spherical particles (Test 1) exhibit the highest void ratio e (defined as the ratio of the volume of voids to the volume of solids) and consequently the lowest compactivity (i.e., packing efficiency) compared to other particle shapes. Conversely, Tests 2 and 4 yield the lowest void ratios, indicating that more cubic-shaped particles result in denser granular packing and higher compactivity. Comparing Tests 2 and 4, both with constant squareness ($\epsilon_1 = 0.6$) but differing sharpness (ϵ_2), the difference in void ratios is relatively minor. In contrast, comparing Tests 2 and 5, where sharpness remains constant ($\epsilon_2 = 0.6$) and squareness (ϵ_1) varies, a significant difference in void ratios is observed. This comparison indicates that squareness (ϵ_1) exerts a stronger influence on granular compactivity than sharpness (ϵ_2). Additionally, when $\epsilon_2 = 0.6$ and ϵ_1 increases from 0.6 to 1.4 (Tests 2

vs. 5), void ratio increases, but this increment is smaller compared to the scenario when $\varepsilon_2 = 1.4$ and ε_1 varies similarly (Tests 4 vs. 3). This suggests that the influence of particle squareness on compactivity becomes more pronounced as particle sharpness increases.

When comparing Test 1 (spheres) to Test 6 (aspect ratio of $AR = 1$ but randomly distributed shape parameters ε_1 and ε_2), the void ratio decreases, indicating that introducing angularity at constant aspect ratio increases packing efficiency. Void ratio decreases further in Test 7, where shape parameters remain constant, but semi-axis ratios are randomly distributed. Finally, in Test 8, where both semi-axis ratios and shape parameters are randomly distributed, compactivity is highest, evidenced by the smallest void ratio. These suggest that the ideal spherical particle tends to maximize void space, whereas more realistic, randomly distributed particle shapes promote tighter packing at constant isotropic stress levels. Furthermore, variations in semi-axis ratios appear to exert a stronger influence on compactivity than variations in shape parameters alone, and randomly distributing all parameters facilitates additional buckling and interlocking among particles, further increasing the compactivity.

Our results highlight particle squareness as the primary shape factor controlling granular compactivity, particularly for particles with higher sharpness, whereas highly spherical particles consistently yield higher void ratios and lower compactivity.

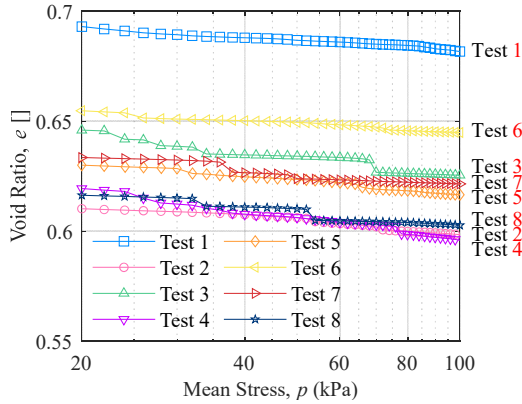


Fig. 4. Isotropic compression curves.

Stress -strain responses of all tests are presented in Fig. 5, and the evolution of the critical-state stress ratio η_c in different specimens is shown in Fig. 6. Comparing Test 1 with Test 7 indicates that randomly distributing the semi-axis lengths has a measurable impact on η_c . However, comparing Test 7 with Test 8 shows almost no difference in η_c , suggesting that once semi-axis lengths are randomized, varying ε_1 and ε_2 does not significantly affect η_c .

Comparing Tests 1 through 6 shows that when the semi-axis ratios remain constant, randomly distributing ε_1 and ε_2 still influences η_c . Tests 2, 3, 4, and 5 all produce similar results that differ from Test 1, implying that ε_1 and ε_2 have similar effects. In particular, $|1 - \varepsilon_j|$ ($j \in [1,2]$) appears to be the key factor in determining their overall influence on η_c .

These findings suggest that aspect ratio has a measurable impact on the critical-state stress ratio and

corresponding shear strength. When aspect ratio is held constant, the sharpness or squareness of particles exerts minimal influence on these parameters, with two key exceptions: (1) perfectly spherical particles (where both sharpness and squareness equal 1); (2) particles whose sharpness and squareness are randomly distributed. In these two cases, the variability in particle shape parameters can lead to noticeable changes in both the critical state and shear strength of the granular assembly.

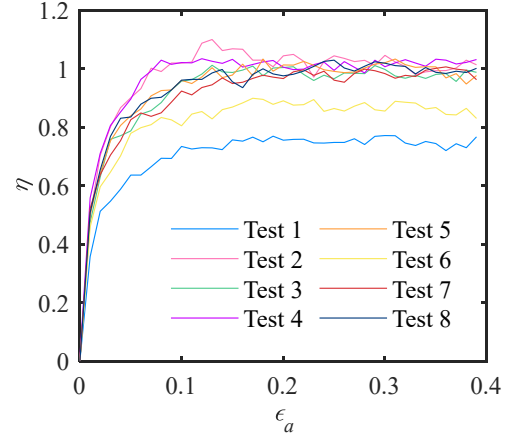


Fig. 5. Stress ratio-axial strain evolution.

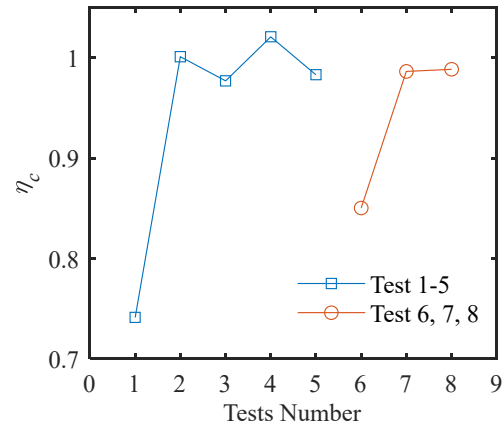


Fig. 6. Evolution of critical state stress ratio

We also consider the microscale effects of changing particle shape. The second-order fabric tensor G_{ij} is calculated according to the contact normals within the granular packing, using the following Equation in [16]:

$$G_{ij} = \frac{2}{N_c} \sum_{c \in C} n_i^c n_j^c \quad (2)$$

where the summation c is performed over all contacts C . It is obvious that $G_{kk} = Z$, the coordination number. The second-order anisotropic fabric tensor F_{ij} is then calculated as:

$$F_{ij} = \frac{15}{2} \left(G_{ij} - \frac{1}{3} G_{kk} \delta_{ij} \right) \quad (3)$$

The degree of fabric anisotropy of the granular assembly is calculated as:

$$F = \frac{\sqrt{\frac{3}{2} F_{ij} F_{ij}}}{Z} \quad (4)$$

The evolution of fabric anisotropy F of Tests 1 through 8 are presented in Fig. 7. Comparisons of F between Tests 1 and 6 reveal relatively minor changes, suggesting that varying the shape parameters ε_1 and ε_2 has a limited effect on fabric anisotropy. In contrast, when comparing Test 7 to Tests 1–6, the impact on F is substantially larger, indicating that changes in the aspect ratio or axis length exert a more pronounced influence on fabric anisotropy than variations in particle sharpness or squareness.

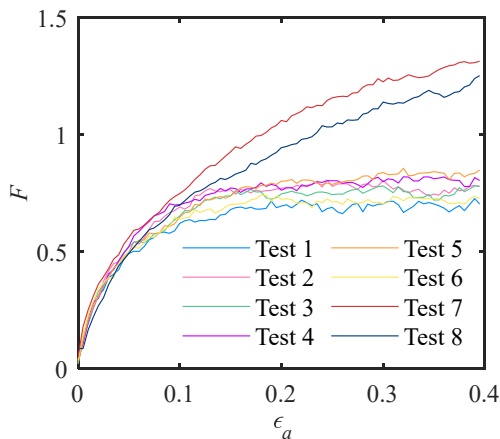


Fig. 7. Evolution of fabric anisotropy.

4 Conclusions

These simulations show that the particle aspect ratio (i.e., the ratio of semi-axes) primarily governs the void ratio (compactivity), critical-state stress ratio (shear strength), and fabric anisotropy in granular assemblies. Spherical particles exhibit higher void ratios and lower shear strength, while more cubic shapes pack more densely, thereby increasing shear strength. Randomly varying the shape parameters associated with sharpness and squareness (ε_1 and ε_2) reduces void ratios and enhances shear strength, but random distributions of aspect ratios have an even more pronounced impact. Sharpness and squareness variations do not significantly affect fabric anisotropy, whereas randomly distributed aspect ratios substantially increase it. Overall, aspect ratio emerges as the dominant factor influencing fabric development, critical-state behavior, and packing efficiency in these simulated granular systems.

References

1. Zhao, J., S. Zhao, and S. Luding, *The role of particle shape in computational modelling of granular matter*. Nature Reviews Physics, 2023. **5**(9): p. 505-525.
2. Xiao, Y., et al., *Effect of Particle Morphology on Strength of Glass Sands*. International Journal of Geomechanics, 2023. **23**(8): p. 04023117.
3. Sandeep Chitta, S., et al., *Influence of Particle Morphology on Angle of Repose Derived from Hopper Flow Tests Using 3D DEM Simulations*, in *Geotechnical Frontiers 2025*. 2025. p. 527-534.
4. Xie, Y.H., et al., *The influence of particle geometry and the intermediate stress ratio on the shear behavior of granular materials*. Granular Matter, 2017. **19**(2): p. 35.
5. Höhner, D., et al., *Comparison of the multi-sphere and polyhedral approach to simulate non-spherical particles within the discrete element method: Influence on temporal force evolution for multiple contacts*. Powder Technology, 2011. **208**(3): p. 643-656.
6. Chen, J., et al., *Effects of particle overall regularity and surface roughness on fabric evolution of granular materials: DEM simulations*. International Journal for Numerical and Analytical Methods in Geomechanics, 2024. **48**(13): p. 3284-3307.
7. Zhao, S., X. Zhou, and W. Liu, *Discrete element simulations of direct shear tests with particle angularity effect*. Granular Matter, 2015. **17**(6): p. 793-806.
8. Lee, S.J., Y.M.A. Hashash, and E.G. Nezami, *Simulation of triaxial compression tests with polyhedral discrete elements*. Computers and Geotechnics, 2012. **43**: p. 92-100.
9. Knowles, J., Y. Ma, and T.M. Evans, *An efficient and robust technique for particulate simulation of arbitrary convex polyhedrons with adaptable material properties*. Computers and Geotechnics, 2023. **155**: p. 105206.
10. Lourakis, M.I.A., *A brief description of the Levenberg-Marquardt algorithm implemented by levmar*. Foundation of Research and Technology, 2005. **4**(1): p. 1-6.
11. Wellmann, C., C. Lillie, and P. Wriggers, *A contact detection algorithm for superellipsoids based on the common - normal concept*. Engineering Computations, 2008. **25**(5): p. 432-442.
12. Gilbert, E.G., D.W. Johnson, and S.S. Keerthi, *A fast procedure for computing the distance between complex objects in three-dimensional space*. IEEE Journal on Robotics and Automation, 1988. **4**(2): p. 193-203.
13. Zhao, S. and J. Zhao, *A poly-superellipsoid-based approach on particle morphology for DEM modeling of granular media*. International Journal for Numerical and Analytical Methods in Geomechanics, 2019. **43**(13): p. 2147-2169.
14. Zhao, S. and J. Zhao, *SudoDEM: Unleashing the predictive power of the discrete element method on simulation for non-spherical granular particles*. Computer Physics Communications, 2021. **259**: p. 107670.
15. Zhao, S., T.M. Evans, and X. Zhou, *Effects of curvature-related DEM contact model on the macro- and micro-mechanical behaviours of granular soils*. Géotechnique, 2018. **68**(12): p. 1085-1098.
16. Wen, Y. and Y. Zhang, *Evidence of a unique critical fabric surface for granular soils*. Géotechnique, 2023. **73**(5): p. 439-454.